Cite as: A. S. Abdelfattah *et al.*, *Science* 10.1126/science.aav6416 (2019).

Bright and photostable chemigenetic indicators for extended in vivo voltage imaging

Ahmed S. Abdelfattah[1]*, Takashi Kawashima[1]*†, Amrita Singh[1,2], Ondrej Novak[1,3], Hui Liu[1], Yichun Shuai[1], Yi-Chieh Huang[4], Luke Campagnola[5], Stephanie C. Seeman[5], Jianing Yu[1], Jihong Zheng[1], Jonathan B. Grimm[1], Ronak Patel[1], Johannes Friedrich[6,7,8], Brett D. Mensh[1], Liam Paninski[6,7], John J. Macklin[1], Gabe J. Murphy[5], Kaspar Podgorski[1], Bei-Jung Lin[4], Tsai-Wen Chen[4], Glenn C. Turner[1], Zhe Liu[1], Minoru Koyama[1], Karel Svoboda[1], Misha B. Ahrens[1]‡, Luke D. Lavis[1]‡, Eric R. Schreiter[1]‡§

[1]Janelia Research Campus, Howard Hughes Medical Institute, Ashburn, VA 20147, USA. [2]Solomon H. Snyder Department of Neuroscience, Johns Hopkins University, Baltimore, MD 21205, USA. [3]Department of Auditory Neuroscience, Institute of Experimental Medicine, Academy of Sciences of the Czech Republic, Prague, Czech Republic. [4]Institute of Neuroscience, National Yang-Ming University, Taipei 112, Taiwan. [5]Allen Institute for Brain Science, Seattle, WA 98109, USA. [6]Department of Statistics and Center for Theoretical Neuroscience, Columbia University, New York, NY 10027, USA. [7]Department of Neuroscience and Grossman Center for the Statistics of Mind, Columbia University, New York, NY 10027, USA. [8]Center for Computational Biology, Flatiron Institute, New York, NY 10010, USA.

*These authors contributed equally to this work.

†Present address: Department of Neurobiology, Weizmann Institute of Science, Rehovot, Israel.

‡These authors contributed equally to this work.

§Corresponding author. Email: schreitere@janelia.hhmi.org

Imaging changes in membrane potential using genetically encoded fluorescent voltage indicators (GEVIs) has great potential for monitoring neuronal activity with high spatial and temporal resolution. Brightness and photostability of fluorescent proteins and rhodopsins have limited the utility of existing GEVIs. We engineered a novel GEVI, "Voltron", that utilizes bright and photostable synthetic dyes instead of protein-based fluorophores, extending the combined duration of imaging and number of neurons imaged simultaneously by more than tenfold relative to existing GEVIs. We used Voltron for in vivo voltage imaging in mice, zebrafish, and fruit flies. In mouse cortex, Voltron allowed single-trial recording of spikes and subthreshold voltage signals from dozens of neurons simultaneously, over 15 min of continuous imaging. In larval zebrafish, Voltron enabled the precise correlation of spike timing with behavior.

Animal behavior is produced by patterns of neuronal activity that span a wide range of spatial and temporal scales. To understand how neural circuits mediate behavior thus requires high-speed recording from ensembles of neurons for long periods of time. Although the activity of large numbers of neurons can now be routinely recorded using genetically encoded calcium indicators (GECIs) (*1*), the slow kinetics of calcium signals complicate the measurement of action potentials, and sub-threshold voltage signals are missed entirely (*1*–*3*). Voltage imaging using genetically encoded voltage indicators (GEVIs) can overcome these challenges, enabling imaging of fast spikes and subthreshold dynamics in genetically defined neurons (*4*, *5*). The high imaging speed and excitation intensity required for voltage imaging, combined with the smaller volume of the cellular membrane, place increased demands on voltage indicators relative to GECIs. Extant GEVIs rely on fluorescence from either microbial rhodopsins (*6*–*8*) or fluorescent proteins (FPs) (*9*–*13*). These fluorophores lack the brightness and photostability to allow in vivo voltage imaging from large fields of view over time scales of many behavioral events, precluding the millisecond-timescale analysis of neural circuits. Improved rhodamine dyes such as the Janelia Fluor® (JF) dyes enable use in complex biological experiments because of their high brightness and photostability (*14*), compatibility with self-labeling protein tags (*15*, *16*), and the ability to traverse the blood-brain barrier for in vivo delivery (*17*). We describe a "chemigenetic", or hybrid protein-small molecule, GEVI scaffold that we call Voltron, which irreversibly binds these synthetic fluorophore dyes. Voltron provides an increased photon yield that enables in vivo imaging of neuronal spiking and subthreshold voltage signals in model organisms with order-of-magnitude improvement in the number of neurons imaged simultaneously over substantially longer

durations.

Our design for a chemigenetic voltage indicator combines a voltage-sensitive microbial rhodopsin domain (*6*, *7*, *11*) with a dye-capture protein domain (Fig. 1A) that irreversibly binds a synthetic fluorophore dye ligand (*14*, *15*) (Fig. 1B), analogous to previously reported voltage indicators that use fluorescent proteins (*10*, *11*, *18*). Transmembrane-voltage-dependent changes in the absorption spectrum (*6*, *19*) of the rhodopsin domain of Voltron reversibly modulate the degree of fluorescence quenching of the nearby bound dye through Förster resonance energy transfer (FRET). We investigated the modularity of this approach, finding that three different rhodopsin domains, QuasAr1 (*7*), QuasAr2 (*7*), and Ace2N (*11*, *20*), modulated the fluorescence of the rhodamine dye Janelia Fluor® 549 (JF_{549}) after binding to either HaloTag (*15*) or SNAP-tag (*21*) dye-capture protein domains (figs. S1 to S8). Removing a small number of amino acid residues at the junction of the rhodopsin and self-labeling tag domains increased the amplitude of fluorescent voltage signals (fig. S1), presumably by decreasing average distance and thus increasing FRET efficiency between the dye and rhodopsin retinal cofactor. The configuration providing the best signal-to-noise ratio for spikes was Ace2N fused to HaloTag with five amino acids removed at their junction (Fig. 1, A and B, and fig. S2), hereafter referred to as Voltron.

We tested several Voltron-dye combinations in cultured rat neurons and acute mouse brain slices with high-speed imaging and simultaneous whole-cell patch clamp electrophysiology (Fig. 1C, figs. S6 and S9 to S13, and tables S1 and S2). Voltron could detect neuronal action potentials and sub-threshold potential changes with a variety of JF dye ligands with emission maxima between 520 nm and 660 nm using fluorescence imaging with one-photon excitation (Fig. 1, C to E, and fig. S6), but was not compatible with two-photon imaging, as described previously for rhodopsin-containing GEVIs (*22*, *23*). Voltron bound to JF_{525} ($Voltron_{525}$) exhibited the highest sensitivity, giving a fluorescence change of –23 ± 1% $\Delta F/F_0$ for a voltage step from –70 mV to +30 mV (Fig. 1E and fig. S9); $Voltron_{549}$ showed similar sensitivity. $Voltron_{525}$ responded to voltage steps with submillisecond on and off time constants (table S3 and fig. S10). We compared the brightness and photostability of Voltron in neuronal cultures with those of two other fluorescent protein-based GEVIs: Ace2N-mNeon (*11*) and ASAP2f (*13*). Both $Voltron_{525}$ and $Voltron_{549}$ were brighter than Ace2N-mNeon (3–4-fold) and ASAP2f (16–18-fold) (Fig. 1F) in cell culture. This difference did not result from differences in expression; we compared the brightness of $Voltron_{549}$ and Ace2N-mNeon at the single-molecule level and observed a similar 3–4-fold brightness difference (Fig. 1G). $Voltron_{525}$ and $Voltron_{549}$ were also more photostable in ensemble measurements (Fig. 1H, tables S4 and S5, and figs. S14 and S15) as well as in single-molecule assays, in which photobleaching times were 8-fold longer for $Voltron_{549}$ than those of Ace2N-mNeon (Fig. 1I). Overall, the improved brightness and photostability of Voltron increased the photon yield by at least 10-fold in neurons over existing GEVIs that rely on fluorescence from FPs.

In vivo, Voltron could be reliably expressed and labeled with dye in mice, larval zebrafish, and adult fruit flies (Figs. 1 to 4 and figs. S16 to S19 and S21 to S45). Simultaneous in vivo electrophysiology and Voltron imaging in each of these organisms confirmed the detection of individual action potentials (Fig. 1, J and K, and figs. S17 to S19). For imaging in the mouse brain, we used a variant of Voltron appended with a 63 amino acid sequence from the rat potassium channel Kv2.1 that restricts expression to the membrane of the cell body and proximal dendrites (*24*, *25*) (Voltron-ST, fig. S20). The rapid kinetics of $Voltron_{525}$-ST allowed clear observation of action potentials in fast-spiking parvalbumin-expressing interneurons in the CA1 region of mouse hippocampus (Fig. 2, A to G, and fig. S21). We measured the orientation tuning of the spiking and subthreshold responses of cortical layer 2/3 pyramidal neurons in mouse primary visual cortex in response to the mouse observing directional movement of light and dark stripes, a benchmark for new indicators (*1*, *11*) (Fig. 2, H to L, and figs. S22 to S24), and confirmed that spiking activity showed sharper orientation selectivity than did subthreshold voltage signals (*26*). We extended the imaging period over several consecutive weeks by injecting additional JF_{525} HaloTag ligand prior to each imaging session (Fig. 2, J to L, and fig. S24).

Next, we attempted to image larger areas containing more neurons for longer times in vivo in mouse cortex (Fig. 3). By widefield microscopy at illumination intensities between 3 and 20 mW/mm^2, we could clearly identify and distinguish action potentials from nearby neurons throughout 15 min of continuous imaging (SNR = 5.3 during the first minute, 4.4 during final minute); (Fig. 3, B to E). We expanded the field-of-view to include dozens of cortical interneurons labeled with $Voltron_{525}$-ST in a transgenic mouse line (NDNF-Cre) (*27*), while imaging at 400 Hz (Fig. 3, F and G, and figs. S25 to S42). Overall, we imaged a total of 449 neurons (12 fields of view in 3 mice), demonstrating routine voltage imaging of populations of neurons in superficial mouse cortex (Fig. 3G and figs. S25 to S42). This scale of in vivo voltage imaging enabled analysis of membrane potential correlations between many neuron pairs (fig. S26).

We used Voltron to image behaving zebrafish larvae, which respond to visual input with fast, directed swim bouts that are tailored to the details of the stimulus (*28*). We sought to uncover how this sensory-to-motor transformation unfolds in neuronal populations at fine timescales that are

inaccessible with calcium imaging. We verified that Voltron could detect action potentials and subthreshold voltage signals in live zebrafish after labeling with several different colors of dye ligands (figs. S17 and S43). We then used Voltron$_{525}$ to monitor neural activity during swim bouts induced by visual motion (Fig. 4A). We recorded Voltron signals from 179 neurons across 43 fish in a motor-sensory nucleus in the tegmental area of the midbrain (Fig. 4B and fig. S44), yielding data on subthreshold membrane voltage modulation as well as automatically-detected spike times (Fig. 4C and fig. S45). We found neuron populations with different temporal activity patterns, including neurons whose firing rate increased ~1 s before the fish started swimming (fig. S44, B and C, "Ramp"), neurons whose firing rate was suppressed each time the fish swam (Fig. 4D, "Off"), and neurons that fired each time the fish swam (Fig. 4D, "Onset" and "Late"). Of the latter types, some fired just before swimming (~20 ms before swim onset, "Onset") and others fired just after swimming (~10 ms after swim onset, "Late"). There was a change in subthreshold voltage that preceded these firing-rate changes by tens of milliseconds (Fig. 4D and fig. S44D). The neuron types were spatially intermingled within this midbrain nucleus (Fig. 4, E and F). The existence of neurons that fired before swimming and neurons that fired after swimming may indicate that this nucleus both partakes in the generation of swim bouts and is influenced by the motor output (Fig. 4G). Thus, Voltron allows for the dissection of population motor coding and sensorimotor integration circuits in ways that neither single-cell electrophysiology nor population calcium imaging can.

We tested Voltron in adult *Drosophila* in vivo by expressing the protein in a pair of dopaminergic neurons, one in each brain hemisphere, which innervate a single compartment in the mushroom body. We detected strong spiking signals from axons and dendrites of these neurons with Voltron$_{549}$ (Fig. 1K and fig. S18). The fluorescence signals matched action potentials detected using electrophysiology. In some neuronal cell types in *Drosophila*, calcium indicators located in the cell body have failed to exhibit fluorescence changes even under conditions where high spike rates are expected (*29*). However, spikes were clearly detectable when imaging from the soma of dopamine neurons with Voltron (fig. S18E). We could clearly distinguish spikes from the two neurons based on the amplitude of the spiking signals even when imaging from neuropil where their axons overlap extensively, likely because each bilaterally-projecting cell contributes a denser innervation of the mushroom body in the ipsilateral hemisphere (fig. S18D).

Combining the molecular specificity of genetically encoded reagents with the superior photophysics of chemical dyes is an established path to improved imaging reagents (*14*). However, previous attempts to create hybrid protein-small molecule indicators by various approaches have not been successful for in vivo imaging (*30*). We engineered a modular sensor scaffold in which the targeting and sensor domains are genetically encoded and only the fluorophore and its protein-binding anchor are synthetic. The resulting chemigenetic indicator, Voltron, exhibits increased photon output, enabling in vivo voltage imaging of many more neurons over longer times—approximately 10^2 more neuron-minutes than other sensors. This improvement enables imaging experiments that can help reveal how the precise electrical dynamics of neuronal populations orchestrate behavior over different time scales.

REFERENCES AND NOTES

1. T. W. Chen, T. J. Wardill, Y. Sun, S. R. Pulver, S. L. Renninger, A. Baohan, E. R. Schreiter, R. A. Kerr, M. B. Orger, V. Jayaraman, L. L. Looger, K. Svoboda, D. S. Kim, Ultrasensitive fluorescent proteins for imaging neuronal activity. *Nature* **499**, 295–300 (2013). doi:10.1038/nature12354 Medline
2. K. Svoboda, W. Denk, D. Kleinfeld, D. W. Tank, In vivo dendritic calcium dynamics in neocortical pyramidal neurons. *Nature* **385**, 161–165 (1997). doi:10.1038/385161a0 Medline
3. V. Emiliani, A. E. Cohen, K. Deisseroth, M. Häusser, All-optical interrogation of neural circuits. *J. Neurosci.* **35**, 13917–13926 (2015). doi:10.1523/JNEUROSCI.2916-15.2015 Medline
4. Y. Xu, P. Zou, A. E. Cohen, Voltage imaging with genetically encoded indicators. *Curr. Opin. Chem. Biol.* **39**, 1–10 (2017). doi:10.1016/j.cbpa.2017.04.005 Medline
5. M. Z. Lin, M. J. Schnitzer, Genetically encoded indicators of neuronal activity. *Nat. Neurosci.* **19**, 1142–1153 (2016). doi:10.1038/nn.4359 Medline
6. J. M. Kralj, A. D. Douglass, D. R. Hochbaum, D. Maclaurin, A. E. Cohen, Optical recording of action potentials in mammalian neurons using a microbial rhodopsin. *Nat. Methods* **9**, 90–95 (2011). doi:10.1038/nmeth.1782 Medline
7. D. R. Hochbaum, Y. Zhao, S. L. Farhi, N. Klapoetke, C. A. Werley, V. Kapoor, P. Zou, J. M. Kralj, D. Maclaurin, N. Smedemark-Margulies, J. L. Saulnier, G. L. Boulting, C. Straub, Y. K. Cho, M. Melkonian, G. K.-S. Wong, D. J. Harrison, V. N. Murthy, B. L. Sabatini, E. S. Boyden, R. E. Campbell, A. E. Cohen, All-optical electrophysiology in mammalian neurons using engineered microbial rhodopsins. *Nat. Methods* **11**, 825–833 (2014). doi:10.1038/nmeth.3000 Medline
8. Y. Adam, J. J. Kim, S. Lou, Y. Zhao, M. E. Xie, D. Brinks, H. Wu, M. A. Mostajo-Radji, S. Kheifets, V. Parot, S. Chettih, K. J. Williams, B. Gmeiner, S. L. Farhi, L. Madisen, E. K. Buchanan, I. Kinsella, D. Zhou, L. Paninski, C. D. Harvey, H. Zeng, P. Arlotta, R. E. Campbell, A. E. Cohen, Voltage imaging and optogenetics reveal behaviour-dependent changes in hippocampal dynamics. *Nature* **569**, 413–417 (2019). doi:10.1038/s41586-019-1166-7
9. L. Jin, Z. Han, J. Platisa, J. R. A. Wooltorton, L. B. Cohen, V. A. Pieribone, Single action potentials and subthreshold electrical events imaged in neurons with a fluorescent protein voltage probe. *Neuron* **75**, 779–785 (2012). doi:10.1016/j.neuron.2012.06.040 Medline
10. P. Zou, Y. Zhao, A. D. Douglass, D. R. Hochbaum, D. Brinks, C. A. Werley, D. J. Harrison, R. E. Campbell, A. E. Cohen, Bright and fast multicoloured voltage reporters via electrochromic FRET. *Nat. Commun.* **5**, 4625 (2014). doi:10.1038/ncomms5625 Medline
11. Y. Gong, C. Huang, J. Z. Li, B. F. Grewe, Y. Zhang, S. Eismann, M. J. Schnitzer, High-speed recording of neural spikes in awake mice and flies with a fluorescent voltage sensor. *Science* **350**, 1361–1366 (2015). doi:10.1126/science.aab0810 Medline

12. A. S. Abdelfattah, S. L. Farhi, Y. Zhao, D. Brinks, P. Zou, A. Ruangkittisakul, J. Platisa, V. A. Pieribone, K. Ballanyi, A. E. Cohen, R. E. Campbell, A Bright and Fast Red Fluorescent Protein Voltage Indicator That Reports Neuronal Activity in Organotypic Brain Slices. *J. Neurosci.* **36**, 2458–2472 (2016). doi:10.1523/JNEUROSCI.3484-15.2016 Medline

13. H. H. H. Yang, F. St-Pierre, X. Sun, X. Ding, M. Z. Lin, T. R. Clandinin, Subcellular Imaging of Voltage and Calcium Signals Reveals Neural Processing In Vivo. *Cell* **166**, 245–257 (2016). doi:10.1016/j.cell.2016.05.031 Medline

14. J. B. Grimm, B. P. English, J. Chen, J. P. Slaughter, Z. Zhang, A. Revyakin, R. Patel, J. J. Macklin, D. Normanno, R. H. Singer, T. Lionnet, L. D. Lavis, A general method to improve fluorophores for live-cell and single-molecule microscopy. *Nat. Methods* **12**, 244–250 (2015). doi:10.1038/nmeth.3256 Medline

15. G. V. Los, L. P. Encell, M. G. McDougall, D. D. Hartzell, N. Karassina, C. Zimprich, M. G. Wood, R. Learish, R. F. Ohana, M. Urh, D. Simpson, J. Mendez, K. Zimmerman, P. Otto, G. Vidugiris, J. Zhu, A. Darzins, D. H. Klaubert, R. F. Bulleit, K. V. Wood, HaloTag: A novel protein labeling technology for cell imaging and protein analysis. *ACS Chem. Biol.* **3**, 373–382 (2008). doi:10.1021/cb800025k Medline

16. L. P. Encell, R. Friedman Ohana, K. Zimmerman, P. Otto, G. Vidugiris, M. G. Wood, G. V. Los, M. G. McDougall, C. Zimprich, N. Karassina, R. D. Learish, R. Hurst, J. Hartnett, S. Wheeler, P. Stecha, J. English, K. Zhao, J. Mendez, H. A. Benink, N. Murphy, D. L. Daniels, M. R. Slater, M. Urh, A. Darzins, D. H. Klaubert, R. F. Bulleit, K. V. Wood, Development of a dehalogenase-based protein fusion tag capable of rapid, selective and covalent attachment to customizable ligands. *Curr. Chem. Genomics* **6**, 55–71 (2012). doi:10.2174/1875397301206010055 Medline

17. J. B. Grimm, A. K. Muthusamy, Y. Liang, T. A. Brown, W. C. Lemon, R. Patel, R. Lu, J. J. Macklin, P. J. Keller, N. Ji, L. D. Lavis, A general method to fine-tune fluorophores for live-cell and in vivo imaging. *Nat. Methods* **14**, 987–994 (2017). doi:10.1038/nmeth.4403 Medline

18. Y. Gong, M. J. Wagner, J. Zhong Li, M. J. Schnitzer, Imaging neural spiking in brain tissue using FRET-opsin protein voltage sensors. *Nat. Commun.* **5**, 3674 (2014). doi:10.1038/ncomms4674 Medline

19. J. M. Kralj, D. R. Hochbaum, A. D. Douglass, A. E. Cohen, Electrical spiking in Escherichia coli probed with a fluorescent voltage-indicating protein. *Science* **333**, 345–348 (2011). doi:10.1126/science.1204763 Medline

20. T. Wada, K. Shimono, T. Kikukawa, M. Hato, N. Shinya, S. Y. Kim, T. Kimura-Someya, M. Shirouzu, J. Tamogami, S. Miyauchi, K.-H. Jung, N. Kamo, S. Yokoyama, Crystal structure of the eukaryotic light-driven proton-pumping rhodopsin, Acetabularia rhodopsin II, from marine alga. *J. Mol. Biol.* **411**, 986–998 (2011). doi:10.1016/j.jmb.2011.06.028 Medline

21. A. Keppler, S. Gendreizig, T. Gronemeyer, H. Pick, H. Vogel, K. Johnsson, A general method for the covalent labeling of fusion proteins with small molecules in vivo. *Nat. Biotechnol.* **21**, 86–89 (2003). doi:10.1038/nbt765 Medline

22. S. Chamberland, H. H. Yang, M. M. Pan, S. W. Evans, S. Guan, M. Chavarha, Y. Yang, C. Salesse, H. Wu, J. C. Wu, T. R. Clandinin, K. Toth, M. Z. Lin, F. St-Pierre, Fast two-photon imaging of subcellular voltage dynamics in neuronal tissue with genetically encoded indicators. *eLife* **6**, e25690 (2017). doi:10.7554/eLife.25690 Medline

23. D. Brinks, A. J. Klein, A. E. Cohen, Two-Photon Lifetime Imaging of Voltage Indicating Proteins as a Probe of Absolute Membrane Voltage. *Biophys. J.* **109**, 914–921 (2015). doi:10.1016/j.bpj.2015.07.038 Medline

24. C. A. Baker, Y. M. Elyada, A. Parra, M. M. L. Bolton, Cellular resolution circuit mapping with temporal-focused excitation of soma-targeted channelrhodopsin. *eLife* **5**, e14193 (2016). doi:10.7554/eLife.14193 Medline

25. S. T. Lim, D. E. Antonucci, R. H. Scannevin, J. S. Trimmer, A novel targeting signal for proximal clustering of the Kv2.1 K+ channel in hippocampal neurons. *Neuron* **25**, 385–397 (2000). doi:10.1016/S0896-6273(00)80902-2 Medline

26. S. L. Smith, I. T. Smith, T. Branco, M. Häusser, Dendritic spikes enhance stimulus selectivity in cortical neurons in vivo. *Nature* **503**, 115–120 (2013). doi:10.1038/nature12600 Medline

27. B. Tasic, V. Menon, T. N. Nguyen, T. K. Kim, T. Jarsky, Z. Yao, B. Levi, L. T. Gray, S. A. Sorensen, T. Dolbeare, D. Bertagnolli, J. Goldy, N. Shapovalova, S. Parry, C. Lee, K. Smith, A. Bernard, L. Madisen, S. M. Sunkin, M. Hawrylycz, C. Koch, H. Zeng, Adult mouse cortical cell taxonomy revealed by single cell transcriptomics. *Nat. Neurosci.* **19**, 335–346 (2016). doi:10.1038/nn.4216 Medline

28. M. B. Ahrens, J. M. Li, M. B. Orger, D. N. Robson, A. F. Schier, F. Engert, R. Portugues, Brain-wide neuronal dynamics during motor adaptation in zebrafish. *Nature* **485**, 471–477 (2012). doi:10.1038/nature11057 Medline

29. T. Hige, Y. Aso, G. M. Rubin, G. C. Turner, Plasticity-driven individualization of olfactory coding in mushroom body output neurons. *Nature* **526**, 258–262 (2015). doi:10.1038/nature15396 Medline

30. A. Wang, J. Feng, Y. Li, P. Zou, Beyond fluorescent proteins: Hybrid and bioluminescent indicators for imaging neural activities. *ACS Chem. Neurosci.* **9**, 639–650 (2018). doi:10.1021/acschemneuro.7b00455 Medline

31. L. A. Gross, G. S. Baird, R. C. Hoffman, K. K. Baldridge, R. Y. Tsien, The structure of the chromophore within DsRed, a red fluorescent protein from coral. *Proc. Natl. Acad. Sci. U.S.A.* **97**, 11990–11995 (2000). doi:10.1073/pnas.97.22.11990 Medline

32. N. C. Shaner, P. A. Steinbach, R. Y. Tsien, A guide to choosing fluorescent proteins. *Nat. Methods* **2**, 905–909 (2005). doi:10.1038/nmeth819 Medline

33. D. Wüstner, T. Christensen, L. M. Solanko, D. Sage, Photobleaching kinetics and time-integrated emission of fluorescent probes in cellular membranes. *Molecules* **19**, 11096–11130 (2014). doi:10.3390/molecules190811096 Medline

34. J. R. Lakowicz, *Principles of Fluorescence Spectroscopy* (Springer, 2006).

35. S. J. Lord, N. R. Conley, H. L. Lee, S. Y. Nishimura, A. K. Pomerantz, K. A. Willets, Z. Lu, H. Wang, N. Liu, R. Samuel, R. Weber, A. Semyonov, M. He, R. J. Twieg, W. E. Moerner, DCDHF fluorophores for single-molecule imaging in cells. *ChemPhysChem* **10**, 55–65 (2009). doi:10.1002/cphc.200800581 Medline

36. C. Eggeling, A. Volkmer, C. A. M. Seidel, Molecular photobleaching kinetics of Rhodamine 6G by one- and two-photon induced confocal fluorescence microscopy. *ChemPhysChem* **6**, 791–804 (2005). doi:10.1002/cphc.200400509 Medline

37. T. J. Wardill, T.-W. Chen, E. R. Schreiter, J. P. Hasseman, G. Tsegaye, B. F. Fosque, R. Behnam, B. C. Shields, M. Ramirez, B. E. Kimmel, R. A. Kerr, V. Jayaraman, L. L. Looger, K. Svoboda, D. S. Kim, A neuron-based screening platform for optimizing genetically-encoded calcium indicators. *PLOS ONE* **8**, e77728 (2013). doi:10.1371/journal.pone.0077728 Medline

38. S. Hippenmeyer, E. Vrieseling, M. Sigrist, T. Portmann, C. Laengle, D. R. Ladle, S. Arber, A developmental switch in the response of DRG neurons to ETS transcription factor signaling. *PLOS Biol.* **3**, e159 (2005). doi:10.1371/journal.pbio.0030159 Medline

39. H. Taniguchi, M. He, P. Wu, S. Kim, R. Paik, K. Sugino, D. Kvitsiani, Y. Fu, J. Lu, Y. Lin, G. Miyoshi, Y. Shima, G. Fishell, S. B. Nelson, Z. J. Huang, A resource of Cre driver lines for genetic targeting of GABAergic neurons in cerebral cortex. *Neuron* **71**, 995–1013 (2011). doi:10.1016/j.neuron.2011.07.026 Medline

40. S. C. Seeman, L. Campagnola, P. A. Davoudian, A. Hoggarth, T. A. Hage, A. Bosma-Moody, C. A. Baker, J. H. Lee, S. Mihalas, C. Teeter, A. L. Ko, J. G. Ojemann, R. P. Gwinn, D. L. Silbergeld, C. Cobbs, J. Phillips, E. Lein, G. Murphy, C. Koch, H. Zeng, T. Jarsky, Sparse recurrent excitatory connectivity in the microcircuit of the adult mouse and human cortex. *eLife* **7**, e37349 (2018). doi:10.7554/eLife.37349 Medline

41. L. Campagnola, M. B. Kratz, P. B. Manis, ACQ4: An open-source software platform for data acquisition and analysis in neurophysiology research. *Front. Neuroinform.* **8**, 3 (2014). doi:10.3389/fninf.2014.00003 Medline

42. D. A. Dombeck, C. D. Harvey, L. Tian, L. L. Looger, D. W. Tank, Functional imaging of hippocampal place cells at cellular resolution during virtual navigation. *Nat. Neurosci.* **13**, 1433–1440 (2010). doi:10.1038/nn.2648 Medline

43. T. Yardeni, M. Eckhaus, H. D. Morris, M. Huizing, S. Hoogstraten-Miller, Retro-orbital injections in mice. *Lab. Anim.* **40**, 155–160 (2011). doi:10.1038/laban0511-155 Medline

44. P. Thévenaz, U. E. Ruttimann, M. Unser, A pyramid approach to subpixel

registration based on intensity. *IEEE Trans. Image Process.* **7**, 27–41 (1998). doi:10.1109/83.650848 Medline

45. T. W. Margrie, A. H. Meyer, A. Caputi, H. Monyer, M. T. Hasan, A. T. Schaefer, W. Denk, M. Brecht, Targeted whole-cell recordings in the mammalian brain in vivo. *Neuron* **39**, 911–918 (2003). doi:10.1016/j.neuron.2003.08.012 Medline
46. F. Franke, R. Quian Quiroga, A. Hierlemann, K. Obermayer, Bayes optimal template matching for spike sorting - combining fisher discriminant analysis with optimal filtering. *J. Comput. Neurosci.* **38**, 439–459 (2015). doi:10.1007/s10827-015-0547-7 Medline
47. R. W. Köster, S. E. Fraser, Tracing transgene expression in living zebrafish embryos. *Dev. Biol.* **233**, 329–346 (2001). doi:10.1006/dbio.2001.0242 Medline
48. R. M. White, A. Sessa, C. Burke, T. Bowman, J. LeBlanc, C. Ceol, C. Bourque, M. Dovey, W. Goessling, C. E. Burns, L. I. Zon, Transparent adult zebrafish as a tool for in vivo transplantation analysis. *Cell Stem Cell* **2**, 183–189 (2008). doi:10.1016/j.stem.2007.11.002 Medline
49. K. Kawakami, H. Takeda, N. Kawakami, M. Kobayashi, N. Matsuda, M. Mishina, A transposon-mediated gene trap approach identifies developmentally regulated genes in zebrafish. *Dev. Cell* **7**, 133–144 (2004). doi:10.1016/j.devcel.2004.06.005 Medline
50. C. Satou, Y. Kimura, H. Hirata, M. L. Suster, K. Kawakami, S. Higashijima, Transgenic tools to characterize neuronal properties of discrete populations of zebrafish neurons. *Development* **140**, 3927–3931 (2013). doi:10.1242/dev.099531 Medline
51. T. Kawashima, M. F. Zwart, C.-T. Yang, B. D. Mensh, M. B. Ahrens, The Serotonergic System Tracks the Outcomes of Actions to Mediate Short-Term Motor Learning. *Cell* **167**, 933–946.e20 (2016). doi:10.1016/j.cell.2016.09.055 Medline
52. N. Vladimirov, Y. Mu, T. Kawashima, D. V. Bennett, C.-T. Yang, L. L. Looger, P. J. Keller, J. Freeman, M. B. Ahrens, Light-sheet functional imaging in fictively behaving zebrafish. *Nat. Methods* **11**, 883–884 (2014). doi:10.1038/nmeth.3040 Medline
53. B. K. Andrásfalvy, G. L. Galiñanes, D. Huber, M. Barbic, J. J. Macklin, K. Susumu, J. B. Delehanty, A. L. Huston, J. K. Makara, I. L. Medintz, Quantum dot-based multiphoton fluorescent pipettes for targeted neuronal electrophysiology. *Nat. Methods* **11**, 1237–1241 (2014). doi:10.1038/nmeth.3146 Medline
54. Y.-K. Bae, S. Kani, T. Shimizu, K. Tanabe, H. Nojima, Y. Kimura, S. Higashijima, M. Hibi, Anatomy of zebrafish cerebellum and screen for mutations affecting its development. *Dev. Biol.* **330**, 406–426 (2009). doi:10.1016/j.ydbio.2009.04.013 Medline
55. M. Takeuchi, K. Matsuda, S. Yamaguchi, K. Asakawa, N. Miyasaka, P. Lal, Y. Yoshihara, A. Koga, K. Kawakami, T. Shimizu, M. Hibi, Establishment of Gal4 transgenic zebrafish lines for analysis of development of cerebellar neural circuitry. *Dev. Biol.* **397**, 1–17 (2015). doi:10.1016/j.ydbio.2014.09.030 Medline
56. M. Guizar-Sicairos, S. T. Thurman, J. R. Fienup, Efficient subpixel image registration algorithms. *Opt. Lett.* **33**, 156–158 (2008). doi:10.1364/OL.33.000156 Medline
57. Y. Aso, D. Hattori, Y. Yu, R. M. Johnston, N. A. Iyer, T.-T. B. Ngo, H. Dionne, L. F. Abbott, R. Axel, H. Tanimoto, G. M. Rubin, The neuronal architecture of the mushroom body provides a logic for associative learning. *eLife* **3**, e04577 (2014). doi:10.7554/eLife.04577 Medline
58. M. Murthy, G. Turner, Dissection of the head cuticle and sheath of living flies for whole-cell patch-clamp recordings in the brain. *Cold Spring Harb. Protoc.* **2013**, 134–139 (2013). Medline
59. R. I. Wilson, G. C. Turner, G. Laurent, Transformation of olfactory representations in the Drosophila antennal lobe. *Science* **303**, 366–370 (2004). doi:10.1126/science.1090782 Medline
60. F. St-Pierre, J. D. Marshall, Y. Yang, Y. Gong, M. J. Schnitzer, M. Z. Lin, High-fidelity optical reporting of neuronal electrical activity with an ultrafast fluorescent voltage sensor. *Nat. Neurosci.* **17**, 884–889 (2014). doi:10.1038/nn.3709 Medline
61. O. Randlett, C. L. Wee, E. A. Naumann, O. Nnaemeka, D. Schoppik, J. E. Fitzgerald, R. Portugues, A. M. B. Lacoste, C. Riegler, F. Engert, A. F. Schier, Whole-brain activity mapping onto a zebrafish brain atlas. *Nat. Methods* **12**, 1039–1046 (2015). doi:10.1038/nmeth.3581 Medline
62. B. A. Wilt, J. E. Fitzgerald, M. J. Schnitzer, Photon shot noise limits on optical detection of neuronal spikes and estimation of spike timing. *Biophys. J.* **104**, 51–62 (2013). doi:10.1016/j.bpj.2012.07.058 Medline

ACKNOWLEDGMENTS

We acknowledge the Janelia Vivarium, Cell Culture, Instrument Design and Fabrication, Imaging, Molecular Biology, and, Virus Production facilities for assistance. Specifically, we would like to thank Brenda Shields, Deepika Walpita, Jim Cox, Chelsea McGlynn, Damien Alcor, Aaron Taylor, Jared Rouchard, Kim Ritola, Xiaorong Zhang and Jordan Towne. We thank Ziqiang Wei for discussions on data analysis. **Funding:** The Howard Hughes Medical Institute (A.S.A., T.K., A.S., O.N., H.L., Y.S., J.Y., J.Z., J.B.G., R.P., B.D.M., J.J.M., K.P., G.C.T., Z.L., M.K., K.S., M.B.A., L.D.L., E.R.S.), Simons Collaboration on the Global Brain Research Awards 325171 (M.B.A., L.P.) and 542943SPI (M.B.A., L.P.), IARPA MICRONS D16PC00003 (L.P.), NIH R01EB22913 (L.P.), Taiwan Ministry of Science and Technology MOST106-2628-B-010-004, MOST105-2628-B-010-005, MOST106-2320-B-010-012 and Taiwan National Health Research Institute NHRI-ex-107-10509NC (T-W.C., B-J.L.), and the Allen Institute for Brain Science (L.C., S.C.S., G.J.M.). **Author contributions:** A.S.A., L.D.L., and E.R.S. conceived the project. A.S.A. engineered Voltron. A.S.A., H.L., J.Z., J.B.G., R.P., J.J.M., Z.L., L.D.L, and E.R.S. performed and analyzed in vitro experiments. T.K., J.F., L.P., M.K., and M.B.A. performed and analyzed experiments in larval zebrafish. A.S., O.N., Y-C.H., L.C., S.C.S., J.Y., G.J.M., K.P., B-J.L., T-W.C., and K.S. performed and analyzed experiments in mouse. Y.S. and G.C.T. performed and analyzed experiments in *Drosophila*. L.P., J.J.M., G.J.M., K.P., B-J.L., T-W.C., G.C.T., Z.L., M.K., K.S., M.B.A., L.D.L., and E.R.S. supervised various aspects of this work. A.S.A. and E.R.S. wrote the manuscript with input and assistance from B.D.M. and all other authors. **Competing interests:** A.S.A, L.D.L. and E.R.S. have filed for a patent on chemigenetic voltage indicators. **Data and materials availability:** All data are available in the manuscript or the supplementary material. Plasmids and AAVs are available from Addgene (https://www.addgene.org), transgenic *Drosophila* stocks are available from the Bloomington Drosophila Stock Center (https://bdsc.indiana.edu), and transgenic zebrafish are available from the Zebrafish International Resource Center (https://zebrafish.org/). J.B.G. and L.D.L. are inventors on U.S. Patent Nos. 9,933,417, 10,018,624, and 10,161,932 as well as U.S. Patent Application No. 16/211,388 held/submitted by the Howard Hughes Medical institute; these cover azetidine-containing fluorophores such as JF525. A.A., L.D.L., and E.R.S. are inventors on patent application WO2018102577A1 submitted by HHMI that covers chemigenetic voltage indicators. DNA plasmids and AAVs, transgenic zebrafish, and transgenic flies described in this manuscript are available from Addgene, ZIRC, and the Bloomington Drosophila Stock Center, respectively, under a material agreement with HHMI.

SUPPLEMENTARY MATERIALS

science.sciencemag.org/cgi/content/full/science.aav6416/DC1
Materials and Methods
Tables S1 to S5
Figs. S1 to S45
References (*31*–*62*)

5 October 2018; accepted 17 July 2019
Published online 1 August 2019
10.1126/science.aav6416

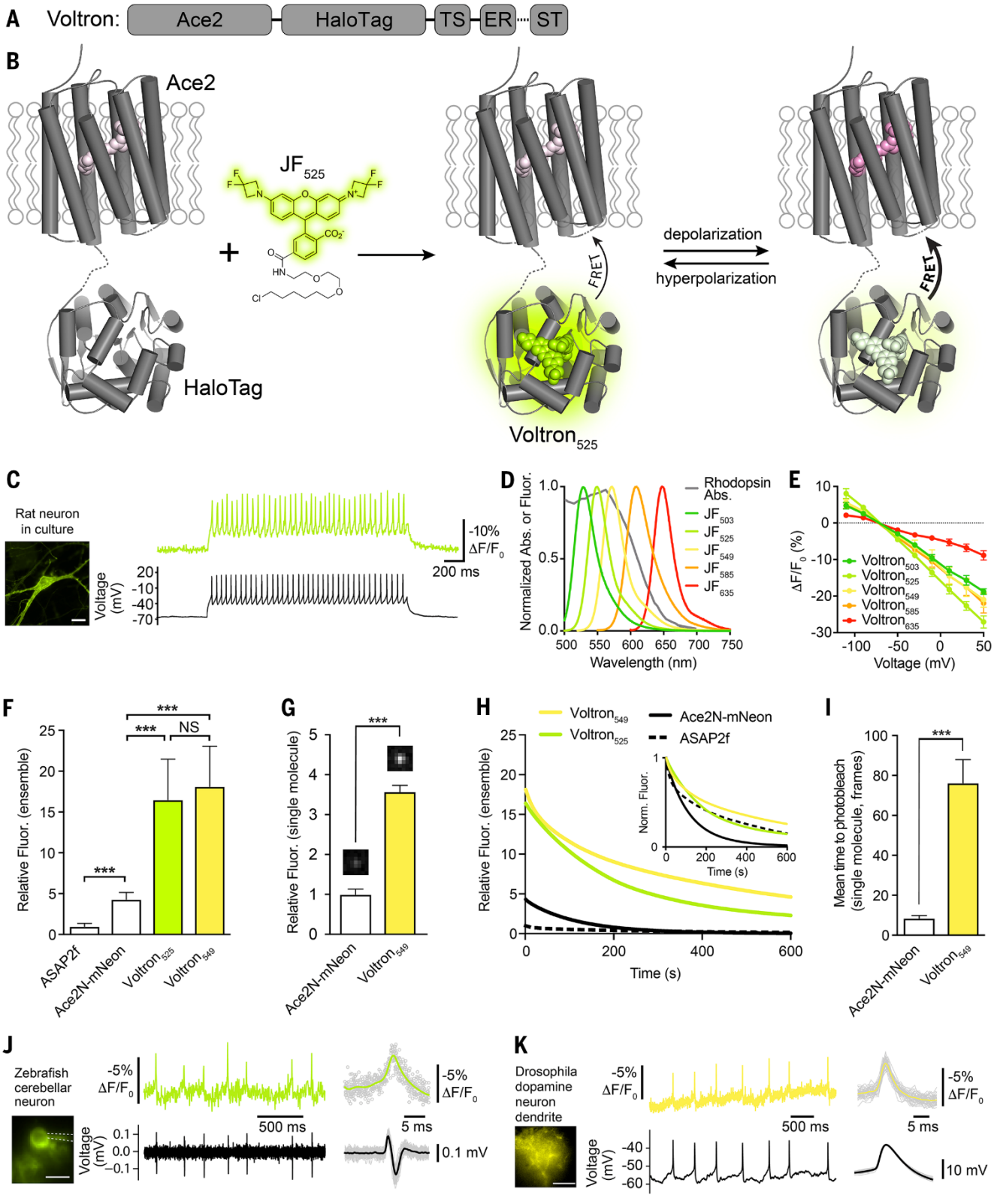

Fig. 1 (preceding page). Development of the chemigenetic voltage indicator Voltron. (**A**) Schematic of Voltron sequence: A rhodopsin (Ace2) is fused to a self-labeling tag domain (HaloTag) with additional sequences added to improve or localize membrane targeting: endoplasmic reticulum export sequence (ER), Golgi export trafficking sequence (TS), and somatic targeting sequence (ST). (**B**) Model of Voltron mechanism. (**C**) Left panel: cultured rat hippocampal neuron expressing Voltron and labeled with JF_{525}. Scale bar: 20 µm. Right panel: single-trial recording of action potentials and subthreshold voltage signals from current injections in primary neuron culture using 400 Hz imaging (top, fluorescence) or electrophysiology (bottom, membrane potential). (**D**) Fluorescence emission spectra of different JF dyes overlaid with the absorbance spectrum of Ace2N. (**E**) Fluorescence change as a function of membrane voltage with different JF dye-Voltron conjugates. (**F**) Relative fluorescence of ASAP2f, Ace2N-mNeon, $Voltron_{525}$ and $Voltron_{549}$ in cultured neurons (n = 70, 68, 48 and 62 measurements from five independent transfections for each construct). Illumination intensity ~10 mW/mm^2 at imaging plane. ***$P < 0.001$, one-way analysis of variance (ANOVA) followed by Bonferroni's test on each pair. Fluorescence was normalized to ASAP2f mean intensity. (**G**) Relative single molecule brightness of Ace2N-mNeon and $Voltron_{549}$. ***$P < 0.001$, two-tailed Student's t-test. (**H**) Bleaching curves for ASAP2f, Ace2N-mNeon, $Voltron_{525}$, and $Voltron_{549}$ in primary neuron culture. Illumination intensity ~23 mW/mm^2 at imaging plane. Bleaching curves were normalized to mean cellular fluorescence from (F) or normalized to the zero-time value (inset). (**I**) Mean time to bleach of Ace2N-mNeon and $Voltron_{549}$ during single-molecule imaging, 100 ms frames. ***$P < 0.001$, two-tailed Student's t-test. (**J** and **K**) Simultaneous in vivo Voltron imaging (300 and 800 Hz, top) and electrophysiology (bottom) in larval zebrafish (extracellular) and adult *Drosophila* (whole-cell), respectively. Spike-triggered averages are shown to the right.

Fig. 2 (next page). Membrane voltage dynamics in hippocampal parvalbumin (PV) neurons and visual cortex pyramidal neurons of mice using Voltron. (**A**) Schematic of imaging of spontaneous activity in the CA1 region of the hippocampus of an awake mouse. (**B**) Image of hippocampal parvalbumin neuron expressing Voltron labeled with JF_{525}. (**C** to **E**) $Voltron_{525}$ raw DF/F_0 traces showing spontaneous spikes of a PV neuron (B) located at a depth of 60 µm in hippocampal CA1 region of a fully awake mouse imaged at 3858 frames per second. Boxes indicate intervals shown at expanded time scales. Scale bar: 20 µm. (**F**) Overlay of 177 spikes detected during a 15 s period (gray) and their average (black). (**G**) Spike shape of 11 PV neurons. (**H**) Schematic of imaging of primary visual cortex of an anesthetized mouse during display of drifting grating visual stimuli. (**I**) Example trace showing 500 Hz Voltron fluorescence during one trial of a sequence of visual stimuli. Arrows below represent the direction of movement of the drifting grating. (**J** to **L**) Top left, images of a pyramidal cell at a depth of 148 µm, imaged three times over a period of four weeks on the indicated weeks after virus injection. Scale bar: 10 µm. Top right, average of all spikes in session (black) and standard deviation (grey). Middle, raw $\Delta F/F_0$ trace for five repetitions in each session, showing two orthogonal orientations (indicated with arrows below) from the neuron pictured on the top left. Bottom, orientation tuning to full-frame drifting gratings of the neuron pictured on the top left, displayed from number of spikes during trials (blue), number of spikes during preceding intertrial intervals (grey), and subthreshold $\Delta F/F_0$ (right y-axis) after low-pass filtering traces using a 10-point median filter. For each orientation, response is calculated by averaging the low-pass filtered trace between 100 – 400 ms after trial onset, and baseline is calculated by averaging the low pass filtered trace from 80 ms preceding trial onset to 20 ms after trial onset. Displayed as response minus baseline. Error bars represent standard error of the mean (s.e.m.) (20 - 22 repetitions per session).

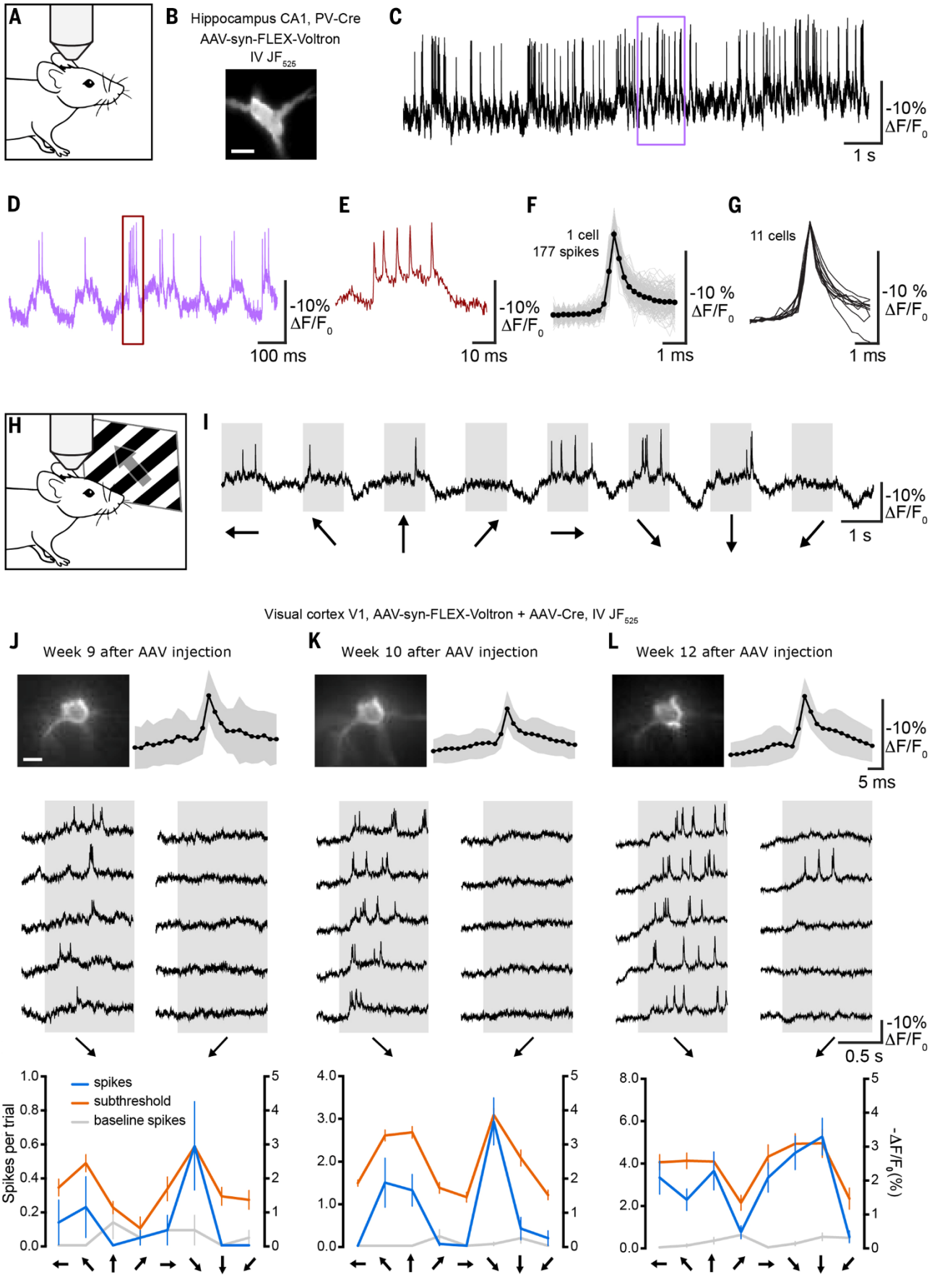

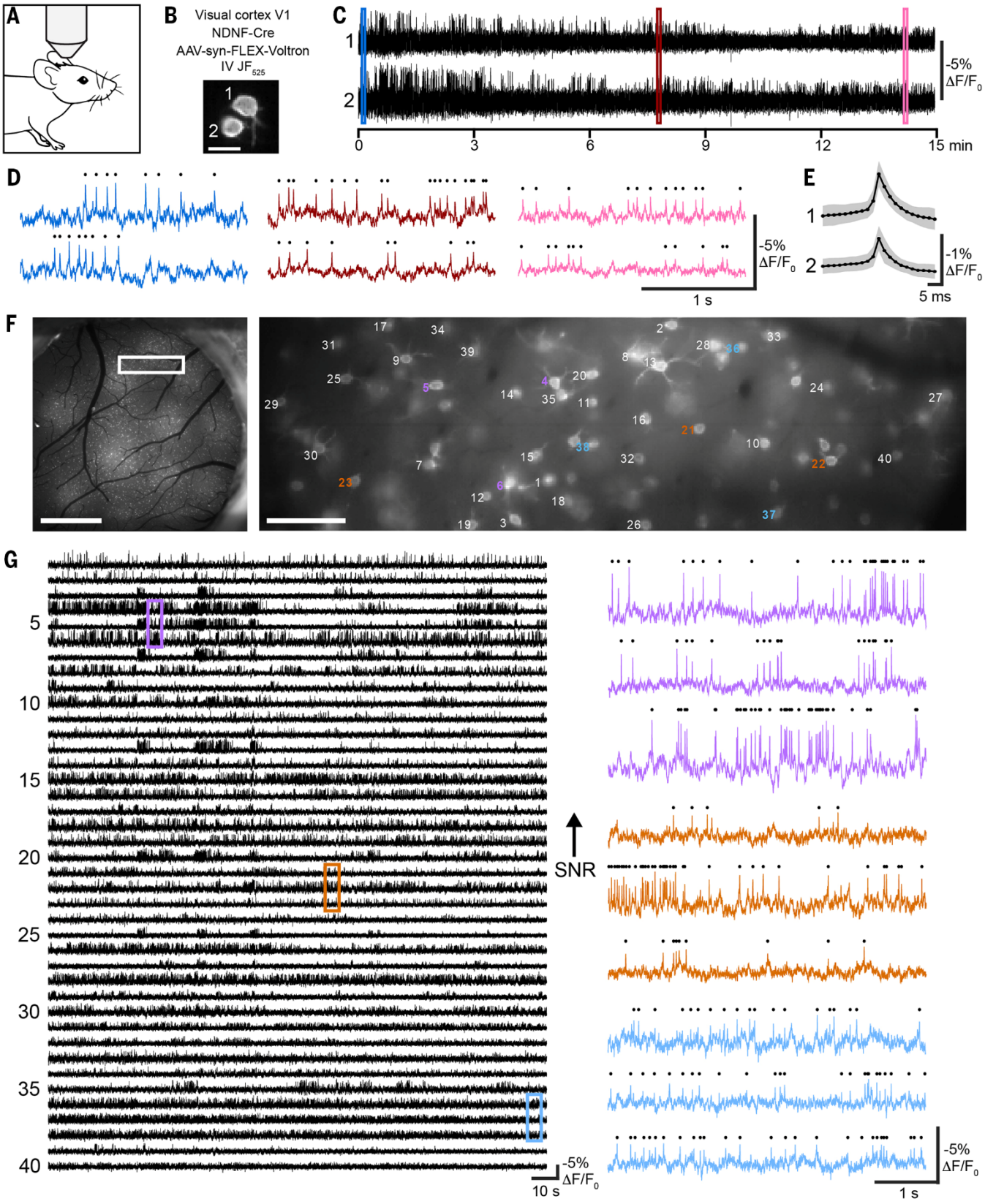

Fig. 3 (preceding page). Long duration and large field-of-view imaging of voltage activity in GABA-ergic neurons in mouse neocortex. (**A**) Schematic of the imaging setup. (**B**) Image of two neurons expressing ST-Voltron$_{525}$ in layer 1 of visual cortex of an NDNF-Cre mouse. Scale bar: 10 μm. (**C**) $\Delta F/F_0$ traces from neurons in (B), recorded over 15 min at 400 Hz. (**D**) Color-coded zooms of indicated regions of the traces in (C) with detected action potentials indicated by black dots above the fluorescence traces. (**E**) Average of all spikes in session (black) and standard deviation (grey). (**F**) Left panel: Fluorescence image of a cranial window over primary visual cortex (V1) in an NDNF-Cre mouse showing Cre-dependent expression of ST-Voltron$_{525}$ (bright spots). Scale bar: 1 mm. Right panel: zoomed image of (F) in the area indicated by the white rectangle, with neurons labels corresponding to fluorescence traces in (G). Scale bar: 100 μm. (**G**) Left panel: $\Delta F/F_0$ traces during 3 min. recording at 400 Hz from neurons pictured in (F), in decreasing order of signal-to-noise ratio. Right panel: zooms of $\Delta F/F_0$ traces from color-coded regions of (G) with detected action potentials represented as black dots above, illustrating representative traces with high (top), medium (middle), and low (bottom) SNR. Traces have been background-subtracted, which removes shared subthreshold membrane potential fluctuations (Supplementary Methods; Compare vs. fig. S25 without subtraction).

Fig. 4 (next page). Voltron reveals millisecond-timescale neural dynamics during swimming behavior in zebrafish. (**A**) Schematic illustration of the setup. An immobilized zebrafish is placed under the light-sheet microscope and the motor signals (inset) from its tail are recorded during the imaging session using a pair of electrodes. Visual stimuli (forward drifting gratings) for triggering swimming responses are presented below the fish. (**B**) Left panel: anatomical location of the imaged brain region (midbrain nucleus; see fig. S44A). Center, a representative field of view of the imaged region expressing Voltron. Scale bar, 20 μm. Right, the position of neurons analyzed in (C). (**C**) Left panel: periods of visual motion (pink) and swim signals (grey) are plotted above Voltron fluorescence traces (black) simultaneously recorded from 11 neurons shown in (B). Right panel: zoom of swimming signals (top) and Voltron fluorescence traces from two representative neurons (bottom) are expanded from the dashed box in the left panel. Dots on the top of each trace represent action potentials recognized by the algorithm described in fig. S45, A and B. Downward triangles and dotted gray lines indicate initiation of each swim bout. (**D**) Mean subthreshold signal (top), mean frequency of action potentials (middle) and raster plots of action potentials (bottom) near the initiation of swim bouts from three representative neurons: "Off" (green), "Onset" (red) and "Late" (blue) neuron. Shadows in the top and middle panels represent s.e.m. across swim events. (**E**) Classification of recorded neurons by their mean subthreshold signals near the initiation of swim bouts. 179 neurons recorded from 43 fish were classified using nonnegative matrix factorization and colored according to the weights for three factors: "onset" (red), "off" (green) and "late" (blue). The details of this classification are described in the Methods. (**F**) Spatial organization of the same population of neurons as in (E). Neurons from multiple fish are superimposed to a single map based on the distance from the center of this midbrain nucleus. (**G**) Hypothetical model of neural activity modulation in this midbrain nucleus.

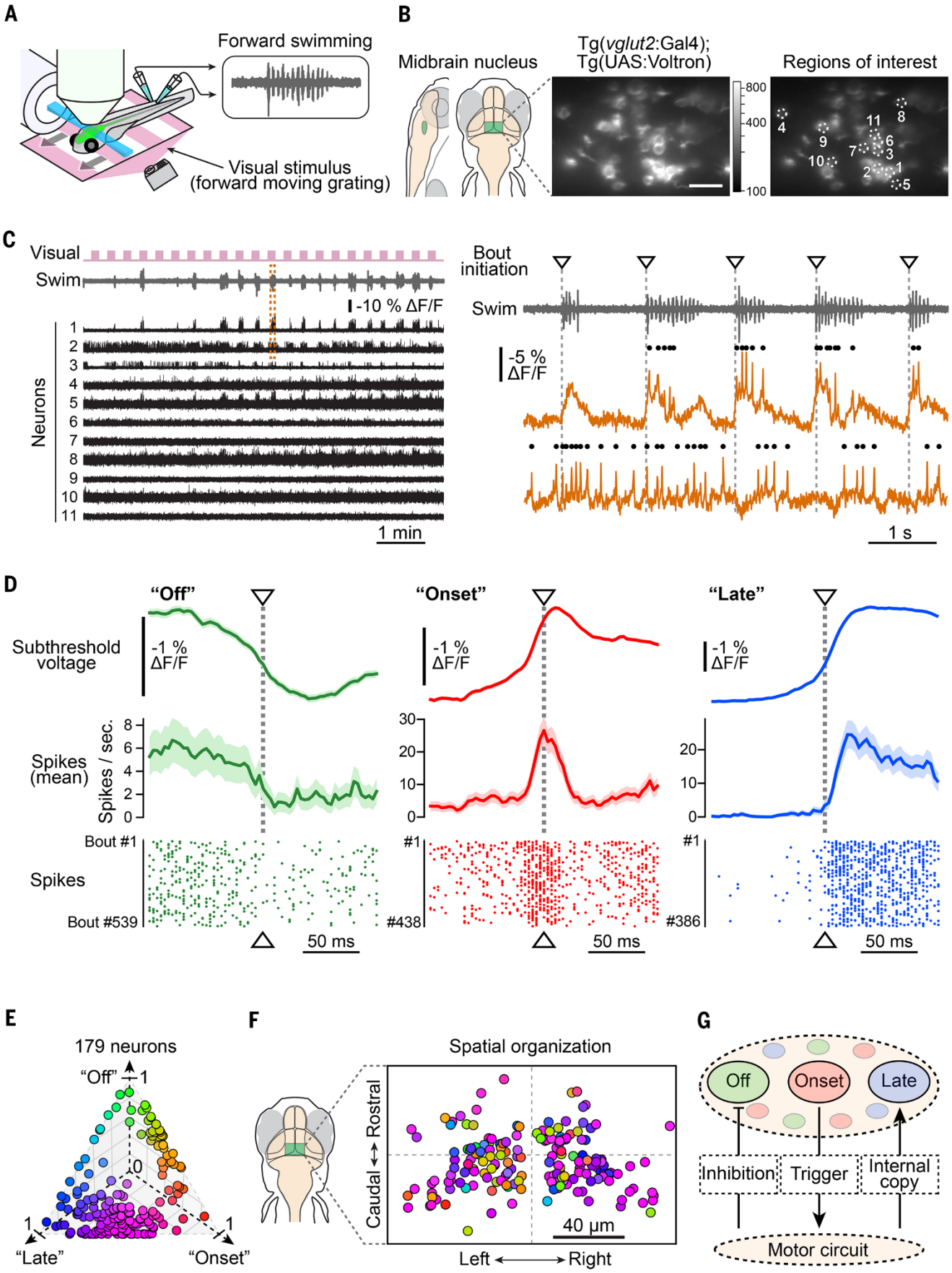

Bright and photostable chemigenetic indicators for extended in vivo voltage imaging

Ahmed S. Abdelfattah, Takashi Kawashima, Amrita Singh, Ondrej Novak, Hui Liu, Yichun Shuai, Yi-Chieh Huang, Luke Campagnola, Stephanie C. Seeman, Jianing Yu, Jihong Zheng, Jonathan B. Grimm, Ronak Patel, Johannes Friedrich, Brett D. Mensh, Liam Paninski, John J. Macklin, Gabe J. Murphy, Kaspar Podgorski, Bei-Jung Lin, Tsai-Wen Chen, Glenn C. Turner, Zhe Liu, Minoru Koyama, Karel Svoboda, Misha B. Ahrens, Luke D. Lavis and Eric R. Schreiter

published online August 1, 2019